NANO LETTERS

2008
Vol. 8, No. 8
2479-2484

# Near-Field Optical Phase Antennas for Long-Range Plasmon Coupling

**Alberto G. Curto and F. Javier García de Abajo***

*Instituto de Óptica, CSIC, Serrano 121, 28006 Madrid, Spain*

*Received May 26, 2008; Revised Manuscript Received June 18, 2008*

**ABSTRACT**

**Plasmon-mediated long-range coupling of optical excitations is shown to be attainable using near-field phase antennas involving nanoparticles situated at focal spots. The antennas rely on metal−surface features that are geometrically arranged to produce constructive interference of plasmons emanating from a source spot over a designated image position. Large image-field intensities and focal spots as narrow as one-third of the wavelength are obtained for source-image separations of tens of micrometers. The ability to strongly couple distant focal spots through phase accumulation produced by engineered plasmon scatterers opens up a vast range of possibilities in contactless plasmon sensing, optical interconnects, and microscopy.**

Surface plasmons hold the promise to become the substitutes of electrical currents in future signal-processing and computing devices, expected to operate at roughly 4 orders of magnitude higher frequencies.[1] In particular, surface plasmon polaritons (SPPs) can couple to light through nanometer-scale metal structures (e.g., gratings and nanoparticles) and then be propagated with tolerable attenuation for hundreds of micrometers. This suggests combining plasmonic logic elements to form complex planar devices extending over that range of distances. In this context, several efficient geometries have been proposed to control plasmon propagation, including rectangular waveguides[2] and channels cut into metal surfaces.[3] Plasmon bands in periodically textured surfaces have also attracted much interest both in one-dimensional[4,5] and in two-dimensional realizations.[6]

A different approach to plasmon interconnects consists in relying on diffraction and interference of surface waves evolving within planar metal regions surrounded by purposely distributed scatterers. Plasmon Bragg mirrors[7] constitute a pioneering example of this idea, in which finite gratings are made to deflect plasmon beams. The plasmon Talbot effect[8] can also produce intense focalization at large distances from a linear periodic array of surface features in a planar metal surface. In a different but related context, optical antennas are being currently investigated to play, in the optical domain, the same role as conventional antennas at much longer wavelengths.[9–11] In another interesting development, the scattering of plasmons by a single particle sitting on a surface has been used to retrieve information on plasmons localized at the particle.[12]

Here, we introduce near-field phase antennas as versatile and controllable systems with a vast range of potential applications that include plasmon interconnects and long-distance sensing. The antennas rely on constructive interference of plasmons emanating from a point source and scattered by a conveniently designed arrangement of features (e.g., holes and dimples) in a plasmon-supporting planar metal surface. We find the field at the image spot to be intense enough to produce significant long-range coupling between localized plasmons of nanoparticles situated at image and source positions (long-range plasmon molecules).

Figure 1a schematically shows the concept behind near-field phase antennas. Plasmons produced at the source (S) are scattered by an array of surface features. The expected position of the image (I) is defined by constructive interference of plasmon signals following geometrical-optics paths and going from the source to each antenna element and from the latter to the image. Although this idea can be realized with more general distributions of surface features (e.g., forming nonrectilinear arrays), we consider for simplicity a nonperiodic linear array along the $x$ axis, separated from both image and source by a distance $a$, and with features situated at positions

$$x_j = \sqrt{(|j| + n_0)^2 \lambda_{SP}^2/4 - a^2} \qquad (1)$$

where $\lambda_{SP}$ is the surface−plasmon wavelength,[13] the sign of the square root is chosen the same as $j$, and $n_0$ is taken such that $x_0 = 0$. The number of antenna elements is $N = 2n + 1$ with $j = -n,...,n$ (see Figure 1). The length difference between paths joining source and image and passing by consecutive antenna elements is precisely $\lambda_{SP}$, and consequently, constructive plasmon interference of all paths considered should occur at the position of the image. Our approach bears strong similarity with Yagi-Uda antennas[14,15] and Fresnel zone lenses, but with both source and image in the vicinities of the antenna.

* Corresponding author. E-mail: jga@cfmac.csic.es.

10.1021/nl801502q CCC: $40.75 
**Published on Web 07/09/2008**

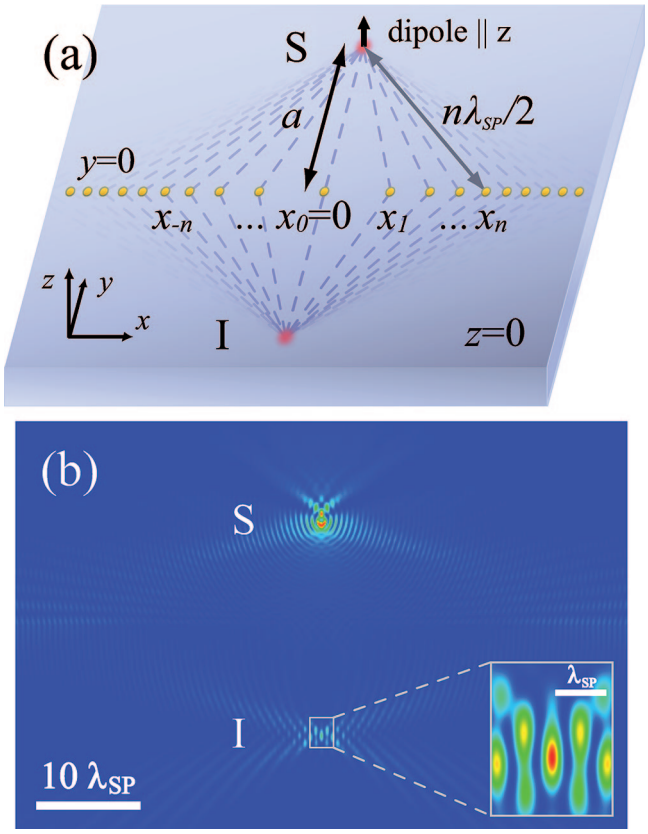


**Figure 1.** (a) Scheme of a near-field phase antenna, whereby plasmons emanating from a point source (S) are scattered by an array of surface features and refocused at an image spot (I). (b) Calculated plasmon-field intensity produced by a unit point-dipole source (S) situated in the upper focal point of an antenna consisting of $N = 721$ dimples of radius $b = 0.15\lambda$ and depth $t = 0.52\lambda$ (this corresponds to point A of Figure 2a). The dimples are drilled in silver, and the light wavelength is $\lambda = 1550$ nm (i.e., $\epsilon_m = -131 + 3.3i$, ref 16, and $\lambda_{SP} = 1544$ nm, ref 13). The distance from both source and image to the antenna is $a \approx 10\lambda_{SP}$. The inset shows a detail of the image focus (I).

The field amplitude of SPPs decays as $1/\sqrt{R}$ away from a point source.[17] This applies in particular to the source of Figure 1a and also to the scattered field produced by each antenna element. Therefore, the in-phase field produced by the array at the image focal spot has the combined amplitude

$$\sum_j \frac{1}{|j| + n_0|\lambda_{SP}} \sim \frac{2}{\lambda_{SP}} \log(N) \qquad (2)$$

which diverges logarithmically with the number of scatterers $N \gg 1$. The magnitude of the image-spot intensity is only limited by finite SPP propagation length and multiple scattering between antenna features.

We describe the response of the antenna scatterers through their dipolar polarizability $\alpha$, assuming that they are sufficiently small to neglect higher-order multipolar corrections (notice that $x_{j+1} - x_j \approx \lambda_{SP}/2$ for $|j| \gg 1$). The induced dipoles excite plasmons that propagate along the surface, but they couple to propagating light waves as well, giving rise to radiative loss of a fraction of the plasmon signal at every scattering event. It should be noted here that a perfect conductor surface can only host parallel magnetic dipoles ($m_x$ and $m_y$) and perpendicular electric dipoles ($p_z$, with $z$ chosen along the surface normal). However, other dipole components can exist in metals of finite conductivity, although their magnitude becomes small when the metal dielectric function takes large values, for example, in noble metals at near-infrared frequencies. We neglect these additional components for simplicity and model the response of each scatterer with dipoles $m_x$, $m_y$, and $p_z$ via the in-plane magnetic polarizability $\alpha_M$ and the perpendicular electric polarizability $\alpha_E$.

The self-consistent response of the array is ruled by the coupled-dipole equation[17]

$$\begin{bmatrix} \alpha_M^{-1} & 0 & 0 \\ 0 & \alpha_M^{-1} & 0 \\ 0 & 0 & \alpha_E^{-1} \end{bmatrix} \begin{bmatrix} m_{xj} \\ m_{yj} \\ p_{zj} \end{bmatrix} = \begin{bmatrix} H^e_{xj} \\ H^e_{yj} \\ E^e_{zj} \end{bmatrix} + \sum_{j' \neq j} \begin{bmatrix} G^{MM}_{xx} & G^{MM}_{xy} & G^{ME}_{xz} \\ G^{MM}_{yx} & G^{MM}_{yy} & G^{ME}_{yz} \\ G^{EM}_{zx} & G^{EM}_{zy} & G^{EE}_{zz} \end{bmatrix} \begin{bmatrix} m_{xj'} \\ m_{yj'} \\ p_{zj'} \end{bmatrix} \qquad (3)$$

where $j$ and $j'$ run over scatterer sites, $E^e$ and $H^e$ denote the source fields in the absence of the antenna, and we approximate the fields produced by unit dipoles at sites $j'$ on scatterer $j$ through [17,18]

$$G^{MM}_{xx} = \pi k^3 B\sqrt{\epsilon_m}[H_0 + H_2(x^2 - y^2)/R^2]$$
$$G^{MM}_{yy} = \pi k^3 B\sqrt{\epsilon_m}[H_0 - H_2(x^2 - y^2)/R^2]$$
$$G^{EE}_{zz} = 2\pi k^3 B[\epsilon_m/(\epsilon_m+1)]^{3/2}\sqrt{1+\epsilon_m}H_0$$
$$G^{MM}_{xy} = G^{MM}_{yx} = \pi k^3 B\sqrt{\epsilon_m}H_2 xy/R^2$$
$$G^{ME}_{xz} = G^{EM}_{zx} = 2\pi i k^3 B(\epsilon_m/\sqrt{\epsilon_m+1})H_1 y/R$$
$$G^{ME}_{yz} = G^{EM}_{zy} = -2\pi i k^3 B(\epsilon_m/\sqrt{\epsilon_m+1})H_1 x/R$$

and $B = (1 - \epsilon_m)^{-1}[\epsilon_m/(1 + \epsilon_m)]^{3/2}$. Here, $H_n \equiv H_n^{(1)}(k_{SP}R)$ is a Hankel function,[19] $R = (x^2 + y^2)^{1/2}$, $(x,y)$ denotes the coordinate vector going from site $j'$ to site $j$, and $k = 2\pi/\lambda$ and $k_{SP}$ are the photon and plasmon wavevectors.

A typical example of focusing by a plasmon phase antenna is shown in Figure 1b. The antenna is formed by $N = 721$ dimples arranged along the $x$ axis at positions given by eq 1. The field intensity takes maximum values near the source (S), where it displays spatial oscillations due to interference between direct dipole emission and reflection from the antenna (an image is also formed at the position of the source because our antenna has mirror symmetry with respect to the $x$ axis). This interference is clearly enhanced where both direct and reflected fields have similar magnitude (i.e., relatively close to the source). Significant plasmon intensity piles up at the image spot (I), approximately 20 SPP wavelengths away from the source and clearly outstanding in a background of lower intensity.

Interestingly, the image focal spot has a width along $x$ close to the diffraction limit, which can be quantified by a fwhm $\sim 0.3\lambda_{SP}$ (see inset in Figure 1b). This is reminiscent of the superoscillation phenomenon, whereby arbitrarily narrow features can result from interference of propagating waves in the far-field.[20,21] The central spot is flanked by

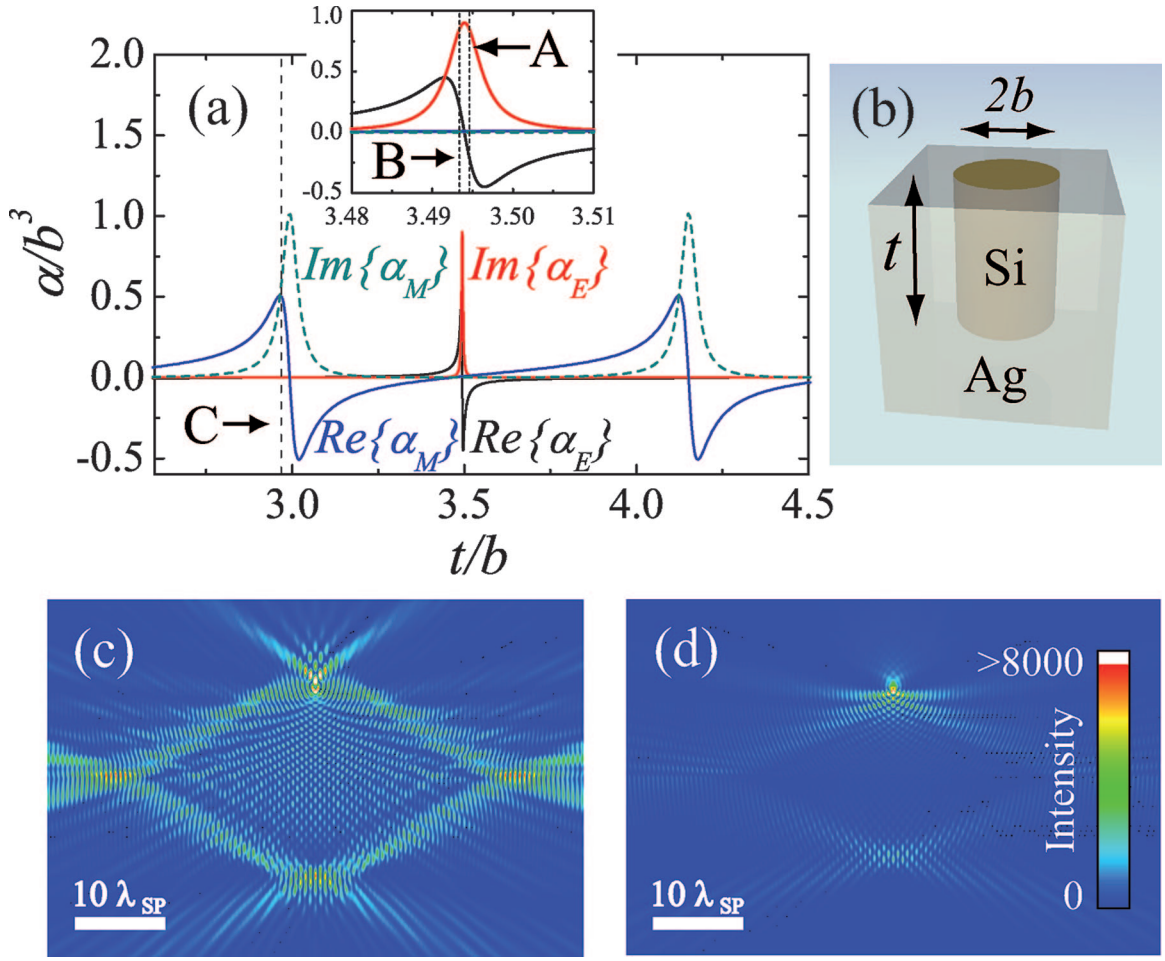


**Figure 2.** (a) In-plane magnetic polarizability $\alpha_M$ and normal electric polarizability $\alpha_E$ of a Si-filled dimple of radius $b$ drilled in a perfect-conductor planar surface as a function of depth $t$. (b) Sketch of a dimple with the geometrical parameters used. (c,d) SPP field intensity for the same antenna as that in Figure 1b (also for $\lambda = 1550$ nm), but with dimples of depth as indicated by labels B and C in part a, respectively. The intensity represents the dimensionless quantity $|E\lambda^3/p|^2$, where $p$ is the unit source dipole. The color scale is linear, with values above 8000 represented in white.

weaker side spots originating in interference between different diffracted waves.

We need strongly scattering antenna elements in order to focus more light to the image spot, because the direct field of the source decays slowly as $1/\sqrt{R}$ on the planar metal surface and thus it is still significant at distant positions from the source dipole. This requires a reliance on resonant scattering that makes our small features optically large. We use in particular small dimples sustaining Fabry−Perot resonances that produce large polarizabilities,[22] and this happens for relatively small radius relative to the wavelength if they are filled with silicon, because the large dielectric function of this material ($\epsilon \sim 12$) shrinks the wavelength inside the dimple cavity. This is shown in Figure 2, where the metal is approximated by a perfect conductor. The polarizability of the dimples has a large impact on the performance of the antennas, as shown in Figure 1b and Figure 2c,d, all of them sharing the same geometrical parameters except the depths of the dimples $t$, which correspond to labels A, B, and C in Figure 2a, respectively. The antennas of Figure 1b and Figure 2c produce intense images, somewhat sharper in the former, whereas the antenna of Figure 2d has a very poor performance. Upon inspection, we have found that large values of $|\alpha_E|$ and small values of $|\alpha_M|$ favor sharper focusing (e.g., see point A in Figure 2a) and reduce the damaging effects of multiple scattering in the array.

A large number of scatterers is important to build up a sufficiently intense image field, according to eq 2. This is illustrated in Figure 3a,b, where the image quality is clearly poorer when the number of antenna elements is reduced from $N = 721$ to $N = 151$ under the conditions of Figure 1b. It should be noted that these antennas can be made to work for a wide range of image−source distances (cf. Figure 3a,c). Finally, the choice of dimple parameters is not unique (cf. Figure 3a,d), although the $|\alpha_M| \ll |\alpha_E|$ condition seems to be essential for achieving good focusing.

We explore in Figure 4 the chromatic performance of the antenna considered in Figure 1b by showing cross section cuts of the image spot along $x$ and $y$ directions. Interestingly, the image intensity is maximum at a slightly red-shifted wavelength with respect to the 1550 nm value used in the antenna design. Besides, the image maximum occurs nearly one wavelength below the ideal position $y = -a$. These effects, which we attribute to deviations from ray optics caused by dynamical diffraction, are familiar in nonparaxial

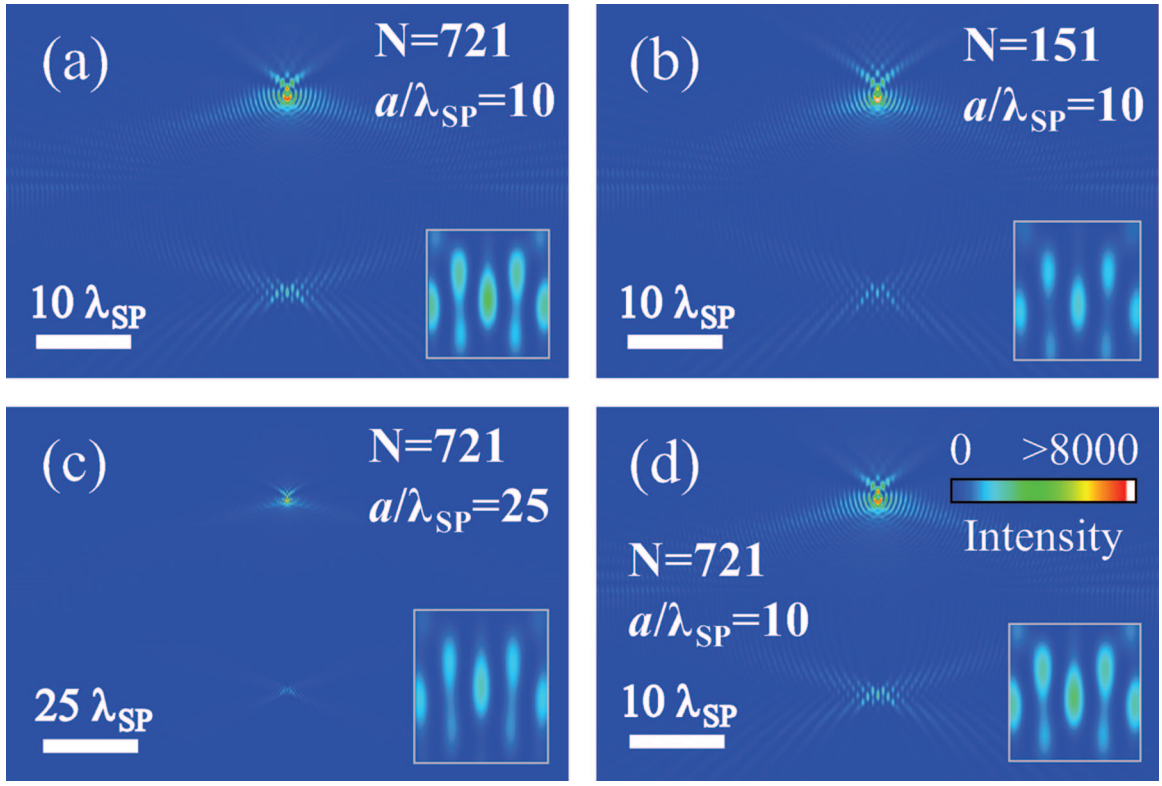


**Figure 3.** SPP intensity of selected phase antennas with different numbers of dimples $N$, image-source distance $2a$, and dimple size for $\lambda = 1550$ nm. The values of $N$ and $a$ are given in text insets. The dimples in a−c are as in Figure 1b (see also point A in Figure 2a). The dimples in part d have radius $b = 0.2\lambda$ and depth $t = 0.94\lambda$. Magnifications of the image region are shown by insets. The color scale is linear, with values above 8000 represented in white.

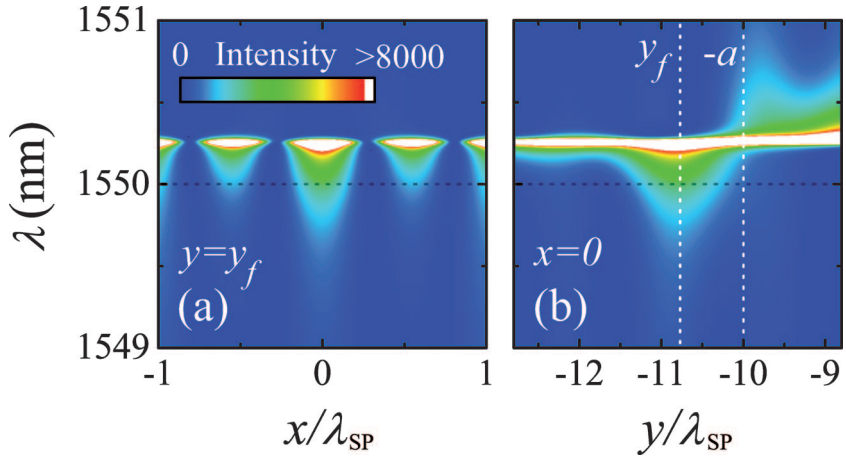


**Figure 4.** Spectral dependence of the SPP image intensity under the same conditions as in Figure 1b for cuts along directions parallel (left, for $y = y_f$ at the intensity maximum) and perpendicular (right, for $x = 0$) with respect to the antenna array. The antenna has been designed to operate at the central wavelength $\lambda = 1550$ nm. The color scale is linear, with values above 8000 represented in white.

discussions of the Talbot effect.[23] Clearly, the antenna has a narrow spectral response that can be advantageous to filter specific wavelengths.

Interestingly, the field intensity at the image is large enough to build up an important back-reaction at the source if an additional scatterer is placed at the image position. To illustrate this concept, we consider two particles capable of sustaining localized plasmon dipole modes oriented perpendicularly with respect to the surface and located at the near-field-antenna focal spots (quantum dots should work equally well to produce similar long-range molecules). The modes of the coupled system are governed by the coupled-dipole equations

$$p_S = \alpha_E^p (G_S p_S + G_I p_I)$$

$$p_I = \alpha_E^p (G_S p_I + G_I p_S)$$

where $\alpha_E^p$ is the electric polarizability of the particles in question, $p_S$ and $p_I$ are the self-consistent dipoles of the two particles, located at source ($y = a$) and image ($y = -a$) spots, respectively, $G_I$ is the normal electric field near the image

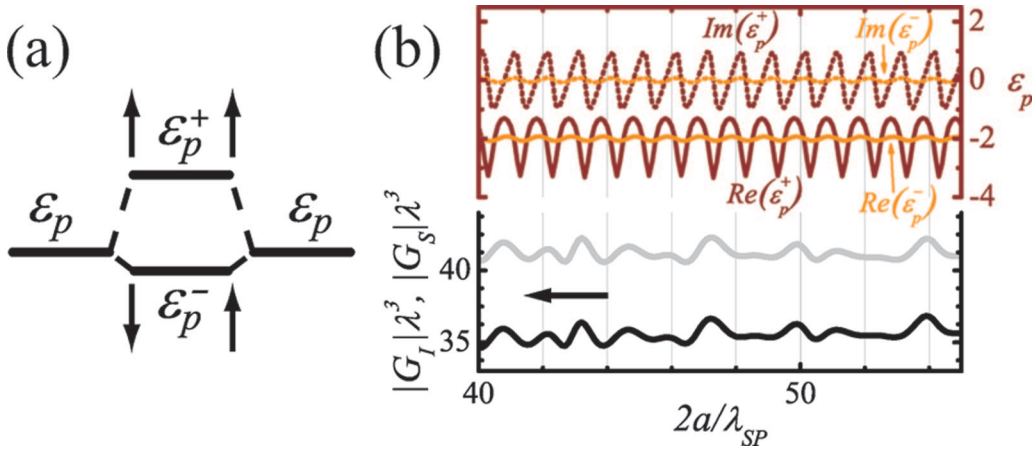


**Figure 5.** (a) Schematic representation of the interaction between two particles located at the focal spots of a near-field phase antenna. When we fix the light wavelength, each particle displays a localized resonance for a given value of its permittivity $\epsilon_P$. When the two particles interact through the antenna, these resonances move to hybridized modes occurring for identical particles of permittivity $\epsilon_p^+$ (symmetric mode) or $\epsilon_p^-$ (antisymmetric mode), with induced dipoles either parallel or antiparallel. (b) Electric field strength (left scale) at the position of both image (total field at $y = -a$, $|G_I|$, black curve) and source (induced field at $y = a$, $|G_S|$, gray curve) as a function of their distance $a$ from an antenna formed by $N = 721$ dimples of radius $b = 0.15\lambda$ and depth $t = 0.52\lambda$ drilled in silver (same parameters as in Figure 1). The operating wavelength is $\lambda = 1550.2$ nm. The right scale shows the resonant permittivities of a particle dimer, as explained in the text.

spot produced by a unit normal electric dipole at the source position, and $G_S$ is the perpendicular field induced on this unit source dipole itself. The dipoles in this symmetric system (identical particles at the same distance from the antenna) must be either parallel ($p_S = +p_I$) or antiparallel ($p_S = -p_I$), subject to the mode conditions $1/\alpha_E^p = G_S + G_I$ and $1/\alpha_E^p = G_S - G_I$, respectively. These conditions depend on the parameters of the particles, as schematically illustrated in Figure 5a, where the single-particle mode occurs for a given value of the particle permittivity $\epsilon_p$, whereas the interaction through the antenna shifts this value to $\epsilon_p^+$ for the symmetric mode and $\epsilon_p^-$ for the antisymmetric one.

We take for simplicity spherical homogeneous particles of permittivity $\epsilon_p$ and radius $R = 194$ nm ($\ll\lambda$), described by their nonretarded polarizability $\alpha_E^p = 2R^3(\epsilon_p - 1)/(\epsilon_p + 2)$. The self-interaction of each particle with the planar metal surface is only introduced through a factor of 2, which accounts for the image dipole in an approximate way, so the particle can be regarded as a model representation of an actual surface feature sustaining localized plasmon modes. In this model, the single-particle dipole-mode condition $\epsilon_p = -2$ shifts to a different value because of interparticle interaction through the antenna.

In particular, Figure 5b shows results for antennas designed to work at $\lambda = 1550$ nm and operating at $\lambda = 1550.2$ nm. The magnitudes of $G_I$ and $G_S$ (see Figure 5b, left scale) are rather large for interparticle separations $2a$ up to tens of SPP wavelengths. Each value of $a$ is of course involving a different geometrical realization of the antenna, with $N = 721$ elements arranged according to eq 1. The difference between $G_I$ and $G_S$ is mainly originating in the direct field of the source, and this difference is small compared with the value of these quantities, thus illustrating the enhancement in interparticle interaction produced by the antenna. The interaction is large enough to produce significant shifts in the symmetric mode, while the antisymmetric mode stays very close to the noninteracting-particles condition. Only values of the resonant permittivity with positive imaginary parts can be realized in practice using passive materials. In particular, we obtain $\epsilon_p^+ = -3.28 + 0.07i$ for particles separated 82.6 $\mu$m (see right scale in Figure 5b). Similar shifts with nearly vanishing imaginary parts of the permittivity are observed for antennas with other interparticle distances, in steps of $\Delta a \sim \lambda_{SP}/2$.

The condition for the antisymmetric mode becomes $1/\alpha_E^p = 0$ if $G_I = G_S$; that is, one recovers the condition for the noninteracting particles, $\epsilon_p = -2$. The actual difference between $G_I$ and $G_S$ is small, and therefore, the antisymmetric mode does not move much from the noninteracting case. The symmetric mode is however exhibiting significant shifts that are clear evidence of the formation of robust long-range dimer plasmon molecules.

In conclusion, we have demonstrated that constructive interference of plasmons scattered by engineered distributions of surface features can produce sharp image spots that are formed micrometers away from the sources. The image fields are intense enough to cause significant refocusing of plasmons back at the source when a plasmon scatterer (e.g., a nanoparticle) is situated at the image spot, thus forming long-range plasmon molecules. These ideas are equally applicable to other types of surface waves like guided modes in planar dielectric waveguides and surface elastic modes. Surface electronic states constitute a suitable platform as well, on which control of interference patterns has been already demonstrated.[24]

Our work opens up the possibility to perform remote optical sensing of molecules located at the source spot by placing a probe at the image focus. More general distributions of surface features could also be employed for long-range plasmon interconnects, in which SPP signals, independently connecting several sources and images, travel along an unstructured region of a planar metal surface, with logical operations being performed in the periphery of that area. One

can also conceive two-dimensional rather than one-dimensional arrangements of surface scatterers, which provide extra degrees of freedom to involve more than two focal spots. Combination of different antennas with scatterers resonating at different frequencies could also offer a solution for near-field multiplexing with a common source spot. Finally, the reported field patterns remain unchanged for micrometers above the surface, except for an overall exponential attenuation,[8] and thus, the observed $\lambda/3$ image spot could find application in subwavelength, pen-light lithography and microscopy.

**Acknowledgment.** We thank Niek Van Hulst and Nikolay Zheludev for stimulating discussions. This work has been supported by the Spanish MEC (NAN2004-08843-C05-05, MAT2007-66050, and consolider NanoLight.es) and by the EU-FP6 (NMP4-2006-016881 "SPANS"). A.G.C. acknowledges funding from a CSIC grant.

## References

(1) Ozbay, E. *Science* **2006**, *311*, 189–193.
(2) Berini, P. *Phys. Rev. B* **2000**, *61*, 10484; **2001**, *63*, 125417.
(3) Bozhevolnyi, S. I.; Volkov, V. S.; Devaux, E.; Laluet, J. Y.; Ebbesen, T. W. *Nature* **2006**, *440*, 508–511.
(4) Ritchie, R. H.; Arakawa, E. T.; Cowan, J. J.; Hamm, R. N. *Phys. Rev. Lett.* **1968**, *21*, 1530–1533.
(5) Heitmann, D. *J. Phys. C* **1977**, *10*, 397–405.
(6) Kitson, S. C.; Barnes, W. L.; Sambles, J. R. *Phys. Rev. Lett.* **1996**, *77*, 2670–2673.
(7) González, M. U.; Stepanov, A. L.; Weeber, J. C.; Hohenau, A.; Dereux, A.; Quidant, R.; Krenn, J. R. *Opt. Lett.* **2007**, *32*, 2704–2706.
(8) Dennis, M. R.; Zheludev, N. I.; García de Abajo, F. J. *Opt. Express* **2007**, *15*, 9692–9700.
(9) Taminiau, T. H.; Moerland, R. J.; Segerink, F. B.; Kuipers, L.; van Hulst, N. F. *Nano Lett.* **2007**, *7*, 28–33.
(10) Novotny, L. *Phys. Rev. Lett.* **2007**, *98*, 266802.
(11) Alaverdyan, Y.; Sepúlveda, B.; Eurenius, L.; Olsson, E.; Käll, M. *Nat. Phys.* **2007**, *3*, 884–889.
(12) Prikulis, J.; Xu, H.; Gunnarsson, L.; Käll, M.; Olin, H. *J. Appl. Phys.* **2002**, *92*, 6211–6214.
(13) Plasmons at the surface of a semi-infinite metal of relative dielectric function $\epsilon_m$ have a wavelength $\lambda_{SP} = \lambda/\mathrm{Re}\{\sqrt{\epsilon_m}/(1+\epsilon_m)\}$, relative to the free-space light wavelength $\lambda$. Here, we concentrate on the situation most likely to find practical application, with small attenuation and $|\epsilon_m| \gg 1$, implying that $\lambda_{SP} \lesssim \lambda$ .
(14) Yagi, H. *Proc. IRE* **1928**, *16*, 715–740.
(15) Li, J.; Salandrino, A.; Engheta, N. *Phys. Rev. B* **2007**, *76*, 245403.
(16) Johnson, P. B.; Christy, R. W. *Phys. Rev. B* **1972**, *6*, 4370–4379.
(17) García de Abajo, F. J. *Rev. Mod. Phys.* **2007**, *79*, 1267–1290.
(18) The actual dipole−dipole interaction involves an integral over all values of the parallel momentum. However, the analytical expressions reported here are obtained in the so-called plasmon-pole approximation,[17,25] in which plasmons are assumed to dominate the interaction.
(19) Abramowitz, M.; Stegun, I. A. *Handbook of Mathematical Functions*; Dover: New York, 1972.
(20) Berry, M. V.; Popescu, S. *J. Phys. A* **2006**, *39*, 6965–6977.
(21) Huang, F. M.; Chen, Y.; García de Abajo, F. J.; Zheludev, N. I. *J. Opt. A-Pure Appl. Opt.* **2007**, *9*, S285–S288.
(22) García de Abajo, F. J.; Sáenz, J. J. *Phys. Rev. Lett.* **2005**, *95*, 233901.
(23) Berry, M. V.; Bodenschatz, E. *J. Mod. Opt.* **1999**, *46*, 349–365.
(24) Manoharan, H. C.; Lutz, C. P.; Eigler, D. M. *Nature* **2000**, *403*, 512–515.
(25) Ford, G. W.; Weber, W. H. *Phys. Rep.* **1984**, *113*, 195–287.

NL801502Q